An updated examination of the Luzon Strait transport

Yi-Chia Hsin,[1] Chau-Ron Wu,[2] and Shenn-Yu Chao[3]

[1]   Despite numerous previous estimates of Luzon Strait transport (LST), we attempt an update using a fine-resolution model. With these improvements, the circulation in and around Luzon Strait shows up rather realistically. Intrusion of a Kuroshio meander into the South China Sea (SCS) is seasonally varying. The LST, especially in the upper ocean, caused by a small difference between the large meander inflow and outflow, is also seasonally varying and subject to large standard deviation. The annual mean LST is estimated to be westward (-4.0 ± 5.1 Sv) along 120.75°E. We have also conducted process of elimination experiments to assess the relative importance of open ocean inflow/outflow, wind stress, and surface heat flux in regulating LST and its seasonality. The East Asian monsoon winds stand out as the predominant forcing. Without it, the upper ocean LST changes from westward to eastward (ranging up to 4 Sv) and, with misaligned seasonality, triggering an inflow from the Mindoro Strait to the SCS to replenish the water mass loss. Discounting monsoon winds, sea level in the Sulu Sea is generally higher because it receives the Indonesian Throughflow before the SCS, which causes an inflow from the Sulu Sea to the SCS. On the other hand, the annual mean wind from the northeast invites outflow from the SCS to the Sulu Sea (or inflow from the Luzon Strait). Weighing the two competing factors together, we see the cessation of northeast monsoon as a condition favorable for the Luzon Strait outflow or the Mindoro Strait inflow.

Citation: Hsin, Y.-C., C.-R. Wu, and S.-Y. Chao (2012), An updated examination of the Luzon Strait transport, *J. Geophys. Res.*, *117*, C03022, doi:10.1029/2011JC007714.

1. Introduction

[2]   The Luzon Strait, the major pathway between the South China Sea (SCS) and the Pacific Ocean, is about 350 km wide and up to about 2500 m deep over the entrance sill along 120.75°E (Figure 1). Its bathymetry, dotted by Batan Islands and Babuyan Islands, is rather complex. The Luzon Strait transport (LST) mixes the SCS and Pacific waters and therefore defines the major characteristics of the northern SCS water [*Wyrtki*, 1961; *Qu et al.*, 2000, 2006b]. Vertically, the mean LST was perceived to be three layered: westward in upper and lower depths and eastward in between. Hydrographic data [*Chen and Huang*, 1996; *Qu*, 2000; *Qu et al.*, 2006a] and lowered Acoustic Doppler Current Profiler (ADCP) measurements [*Tian et al.*, 2006; *Yang et al.*, 2010] bear this out.

[3]   The varying degree of Kuroshio encroachment and, in the extreme, intrusion from east of the strait influences the magnitude and seasonality of LST. The mechanism leading to the Kuroshio intrusion and LST has drawn considerable

attention. In our view, the investigations appear to be on the right track, but the source mechanism may still elude us. Phenomenologically, the meridional pressure difference across the strait, higher to the north on average, could be related to the degree of Kuroshio intrusion and LST [*Qu*, 2000]. In an attempt to trace back farther to the source, this meridional pressure gradient could be related to the low sea surface height west of the Luzon Island, which, according to *Liang et al.* [2008], is attributed to the local wind stress curl inside the SCS. *Metzger and Hurlburt* [1996] attributed the seasonal variation of LST, but not the mean, to the pileup of waters by monsoon winds both inside and outside the SCS. Their subsequent investigations [*Metzger and Hurlburt*, 2001a; *Metzger*, 2003] pointed out the model sensitivity to the local bathymetry and coastline resolution. More recently, *Zhao et al.* [2009] attributed the mean LST to the Pacific basin-scale wind field instead of the SCS monsoon winds. In summary, whether the Kuroshio intrusion and LST are driven by winds inside or outside the SCS or both continues to be a source of attention.

[4]   The seminal work of *Wyrtki* [1961] seemed to attract subsequent estimates of LST. The Kuroshio encroachment or intrusion produces westward inflow from southern channels of the Luzon Strait and eastward outflow farther north. Direct estimates of LST as a small difference between large inflow and outflow are by no means trivial and are subject to considerable uncertainties. Indirectly, some estimate LST as the residual after summing up inflows and outflows through

_____

[1]Department of Oceanography, University of Hawaii at Mānoa, Honolulu, Hawaii, USA.
[2]Department of Earth Sciences, National Taiwan Normal University, Taipei, Taiwan.
[3]Horn Point Laboratory, University of Maryland Center for Environmental Science, Cambridge, Maryland, USA.
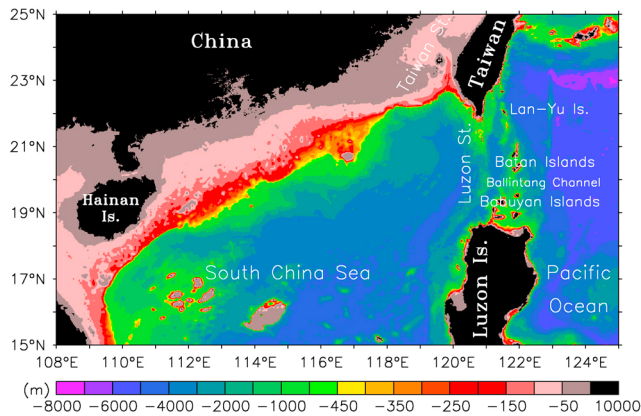
Figure 1. Bathymetry of the northern South China Sea.

all other openings of the SCS, excluding river inputs and sea surface evaporation and precipitation. Tables 1, 2, and 3 summarize results from long-term observations, numerical models, and short-term cruise data, respectively. On the basis of the long-term observational data (Table 1), the mean LST was between 3 and 6.5 Sv westward (1 Sv = 10^6 m^3 s^{-1}), far exceeding the original estimate of 0.5 Sv by *Wyrtki* [1961]. Model estimates (Table 2) range larger (between 0.6 and 10.2 Sv westward), understandably due to differences in grid resolution, topography representation, and computation methodology. Estimates based on short-term cruises (Table 3) are also subject to large uncertainties but often reveal the three-layered structure of LST [*Tian et al.*, 2006; *Yuan et al.*, 2008a, 2009].

[5] Tables 1 and 2 also reveal the seasonal variability of LST. According to historical hydrographic data, the LST is larger in winter and smaller in summer [*Wyrtki*, 1961; *Shaw*, 1989, 1991; *Qu*, 2000]. *Shaw* [1989] likened the variability to the degree of Kuroshio intrusion, which starts in late summer, peaks in winter, and ceases by late spring. By analyzing the historical temperature and salinity profiles of *Levitus and Boyer* [1994] and *Levitus et al.* [1994], LST in the upper 400 m is consistently westward; it is 3 Sv when averaged over a year, peaking to 5.3 Sv in January–February

and bottoming out to 0.2 Sv in June–July [*Qu*, 2000]. Numerical models also reveal a similar seasonality. For example, *Metzger and Hurlburt* [1996] suggested that the westward LST is the largest (8 Sv) in November and smallest (0.5 Sv) in June. Seasonal reversal of the East Asia monsoon, high summer insolation, and variability in the large-scale planetary wind may all contribute to the seasonality. This is one of the factors motivating us to investigate further.

[6] Previous model estimates, each having its strength and weakness, bridge observation gaps and put the subject in perspective. Global models [*Metzger and Hurlburt*, 1996; *Wajsowicz*, 1999; *Qu et al.*, 2004; *Song*, 2006; *Wang et al.*, 2006; *Yaremchuk et al.*, 2009] were necessarily coarse in resolution. Some truncated surrounding shallow seas [*Metzger and Hurlburt*, 1996; *Wajsowicz*, 1999; *Qu et al.*, 2004; *Wang et al.*, 2006; *Yaremchuk et al.*, 2009]. Regional models, among which some keep the channels around SCS open [e.g., *Xue et al.*, 2004] and some close parts of channels [e.g., *Metzger and Hurlburt*, 2001b; *Metzger*, 2003], thrived on improved grid resolution but depended on annual or monthly climatology winds. Instead of climatology winds, *Liang et al.* [2008] adopted a quarter-degree western Pacific model (20.8°S–45.1°N and 95°E–160°E) driven by 1996–2001 European Centre for Medium-Range Weather Forecasts (ECMWF) monthly winds to address the LST variation. Although their model kept the channels around the SCS open, the closed model domain boundaries preclude basin-scale fluctuations in the Pacific from entering the domain [*Liang et al.*, 2008, Figure 10]. The present work takes steps forward by combining finer model grids, refined topography representation and improved spatiotemporal resolution in atmospheric forcing (6 h interval and half degree resolution of the satellite-based wind product). We also keep all the lateral boundaries open, allowing basin-scale variations to come in from the lateral boundaries. We conduct process of elimination experiments to assess the relative importance among several major forces and offer a renewed examination of LST. Section 2 describes the observation-validated, East Asian Marginal Seas model and several side experiments. Section 3 shows main results. Section 4 uses the series of side experiments

Table 1. Summary of Luzon Strait Transport Based on Long-Term Observational Data[a]

	ANN	SPR	SUM	AUT	WIN	Method
Wyrtki [1961]	−0.5	0	2.75	−0.5	−2.75	dynamic method[b] (0–175 m)
Chu and Li [2000]	−6.5			−1.4 (Sep)	−13.7 (Feb)	GDEM[c], P vector method[d]
Qu [2000]	−3.0		−0.2		−5.3	dynamic method (400 dbar)
Qu et al. [2000]	−4					island rule[e]
Liang et al. [2003]	−3					Sb-ADCP[f] (0–300 m)
Lan et al. [2004]		−2.5 (Apr)	−0.29 (Jul)	−2.44 (Oct)	−5.53 (Jan)	GDEM, P vector method, 0 to bottom
Lan et al. [2004]		−1.31 (Apr)	1.01 (Jul)	−1.75 (Oct)	−3.98 (Jan)	GDEM, P vector method, 0–500 m
Su [2004]	−4.2 to −5.0					mass balance of historical values[g]
Yaremchuk and Qu [2004]	−3		−1.2		−4.8	diagnostic method[h]

[a]Positive eastward and negative westward transport (in Sv). ANN, annual; SPR, spring; SUM, summer; AUT, autumn; WIN, winter.
[b]Geostrophic transport derived from hydrographic data.
[c]Navy's Global Digital Environmental Model data set.
[d]Inverse calculation of geostrophic velocity [*Chu*, 1995].
[e]Integrating wind stress over a closed path to derive transport as in the work by *Qu et al.* [2000].
[f]Shipboard Acoustic Doppler Current Profiler.
[g]Using the historical transport values of other straits around the SCS to derive the Luzon Strait transport.
[h]An extension of dynamic method using hydrostatic balance, continuity, and conservation of potential temperature, salinity, and momentum.

Table 2. Summary of Luzon Strait Transport Based on Models[a]

	ANN	SPR	SUM	AUT	WIN	Note
Metzger and Hurlburt [1996]	−2.4–−4.4					1/2° global NLOM[b]
Wajsowicz [1999]	−2.85					0.4° global POCM[c] (1987–1995)
Lebedev and Yaremchuk [2000]			−4.7		−6.3	1/6° OGCM[d]
Metzger and Hurlburt [2001b]	−1.8					1/8° North Pacific NLOM
Metzger [2003]	−0.6–−1.3					1/16° North Pacific NLOM
Qu et al. [2004]	−2.4		0.9 (Jun)		−6.1 (Jan)	1/4° MOM2[e]
Fang et al. [2005]	−4.37	−4.78	−1.87	−3.36	−7.47	1/6° MOM2
Song [2006]	−10.2		−8.2		−12.2	1/3°–1/2° global model
Wang et al. [2006]	−1.5					1/2° SODA[f] (1958–2004)
Rong et al. [2007]		−0.74			−3.1	1/2° SODA (1958 ∼ 2004)
Wang et al. [2009]	−4.5		−2.1		−7.6	1/4°–2° quasi-global HYCOM[g]
Yaremchuk et al. [2009]	−2.4	−2.1	−0.7	−2.9	−4	1/2° reduced gravity model with data assimilation, 0–700 m
Zhao et al. [2009]	−5.7	−2.6	−1.0	−9.0	−8.1	1/4°–2° regional POM[h]

[a]Positive eastward and negative westward transport (in Sv). ANN, annual; SPR, spring; SUM, summer; AUT, autumn; WIN, winter.
[b]Naval Research Laboratory Layered Ocean Model.
[c]Parallel Ocean Climate Model based on the Bryan-Cox model.
[d]Ocean General Circulation Model based on the Bryan-Cox model.
[e]Modular Ocean Model version 2.
[f]Simple Ocean Data Assimilation data set.
[g]Hybrid Coordinate Ocean Model.
[h]Princeton Ocean Model.

to identify major forcing regulating the LST. Section 5 presents discussion and conclusions.

2. Model Description and Thought Experiments

[7] The East Asian Marginal Seas (EAMS) model used in this study is based on the Princeton Ocean Model [*Mellor*, 2004]. On the basis of hydrostatic approximation, this model solves three-dimensional primitive equations for the momentum, salt, and heat and evaluates turbulence by the level 2.5 Mellor-Yamada scheme. The model covers a

domain of 99°E–140°E and 0°–42°N (boxed area in Figure 2) with a horizontal resolution of 1/8° × 1/8° and has 26 sigma levels in the vertical. On open boundaries (the thick lines in Figure 2), its lateral boundary conditions are one-way nested in a 1/4° × 1/4° North Pacific Ocean (NPO) model having an expanded domain of 99°E–71°W and 30°S–65°N (Figure 2). The daily outputs of NPO model are linearly interpolated in space and time to the open boundaries of EAMS model. Details about the one-way nesting were given by *Wu and Hsin* [2005]. The NPO model is initially spun up for 50 years. The initial spin-up is driven by

Table 3. Summary of Luzon Strait Transport Based on Short-Term Observational Data[a]

	Transport (Sv) (Depth Range (m))	Method	Exploration Time
Tian et al. [2006]	−6 (0 to bottom) −9 (0–500) 5 (500–1500) −2 (>1500)	lowered ADCP[b]	4–6 Oct 2005
Liao et al. [2008]	−10.3 (0–400) −7.2 (0–2000)	dynamic method[c]	28 Nov to 27 Dec 1998
Yuan et al. [2008a]	−3.5 (0 to bottom) −3.5 (0–400) 0.22 (400–1200) −0.22 (1200 to bottom)	diagnostic method[d]	28 Aug to 10 Sep 1994
Yuan et al. [2008b]	−0.8 (0–400) 2.4 (500–1200)	diagnostic method	Mar–Apr 2002
Yuan et al. [2009]	−3 (0 to bottom) −6.6 (0–400) 3.7 (400–2000) −0.1 (2000 to bottom)	diagnostic method	8–27 Mar 1992
Zhou et al. [2009]	−3.25 (0–1500) −4.47 (0–500) 1.12 (500–1500)	dynamic method	18–20 Sep 2006
Yang et al. [2010]	5.5(0–bottom) 5 (0–500) 2.5 (500–1500) −2 (1500 to bottom)	lowered ADCP	5–14 Jul 2007

[a]Positive eastward.
[b]Acoustic Doppler Current Profiler.
[c]Geostrophic transport derived from hydrographic data.
[d]An extension of dynamic method using hydrostatic balance, continuity, and conservation of potential temperature, salinity, and momentum.
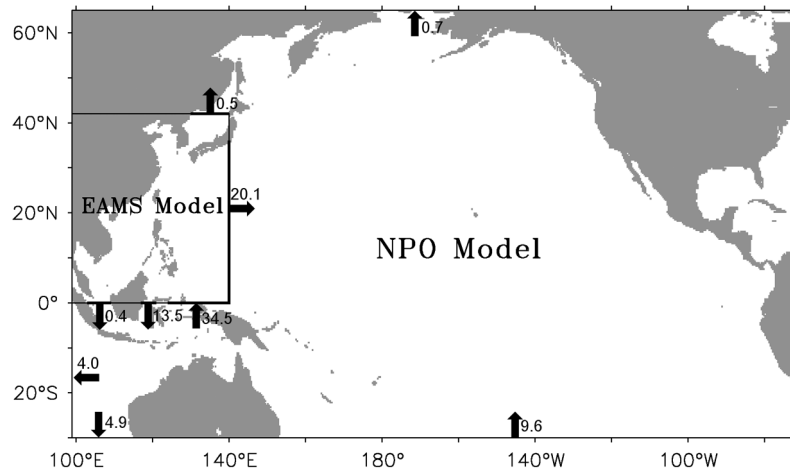
Figure 2. Nested East Asian Marginal Seas model (EAMS) domain within the North Pacific Ocean (NPO) model. The 10 year (1999–2008) mean volumetric fluxes in and out of open ocean boundaries are indicated by thick arrows and numbers (in Sv).

monthly $2.5° \times 2.5°$ NCEP-DOE 10 m wind climatology derived from averaging all historical data month by month regardless of the year (http://www.esrl.noaa.gov/psd/data). Also, the monthly climatology of the Simple Ocean Data Assimilation (SODA) reanalysis products, similarly derived through averaging over all available years with $0.5°$ resolution (http://apdrc.soest.hawaii.edu/), provide lateral boundary conditions for the NPO model. This type of monthly climatology precludes interannual variations and fluctuations below the monthly time scale. To activate interannual and intramonthly variations, we subsequently drive the NPO model with 6 hourly NCEP-DOE reanalysis surface winds from 1948 to 2008. Concurrently, the monthly SODA data, now varying from year to year, provide the open boundary conditions for the model. Annual mean transports through open boundaries of NPO model are labeled in Figure 2. In the southwest corner of the NPO domain, the mean transport is about 9 Sv, corresponding to the transport of Indonesian Throughflow estimated from 20 year expendable bathythermography data [*Wijffels et al.*, 2008].

[8] The topography of EAMS model is a blend of the $1/30° \times 1/30°$ TaiDBMv6 (Ocean Data Bank, Nation Center for Ocean Research, Taiwan) and $1/12° \times 1/12°$ ETOPO5 (National Geophysical Data Center, NOAA, National Environmental Satellite, Data and Information Service) bathymetric data. At the sea surface, it is forced by the 6 hourly $0.5° \times 0.5°$ QuikSCAT/NCEP blended wind product from the Data Support Section of the Computational and Information Systems Laboratory at the National Center for Atmospheric Research (http://dss.ucar.edu), and heated (or cooled) by the 6 hourly $2.5° \times 2.5°$ NCEP-DOE reanalysis II heat flux data set. The last version of this model prescribed the observed temperature distribution at sea surface and was able to reproduce variations of Taiwan Strait currents [*Wu and Hsin*, 2005] and the Kuroshio below and beyond seasonal time scale [*Hsin et al.*, 2008; *Wu et al.*, 2008; *Hsin et al.*, 2010; *Sheu et al.*, 2010]. In this work, we changed the surface thermal boundary condition from prescribed temperature distributions to heat flux specifications. This allows us to examine how surface heat flux affects LST.

[9] Forced by 6 hourly wind stress, 6 hourly sea surface heat fluxes (including sensible heat flux, latent heat flux, and shortwave flux), and daily lateral boundary conditions, the control run (CTL in Table 4) describes the mean state and seasonal variability of circulation around the Luzon Strait. We then use four additional experiments to distinguish effects of time-varying open ocean influences, winds, and surface heat fluxes on LST. Table 4 summarizes the model design of wind stress, heat flux, and open ocean boundary conditions for each experiment. Simplifying to the extreme, experiment NO fixes open ocean boundary conditions at the 10 year (1999–2008) mean from NPO model and removes wind forcing and surface heat flux, thus leaving the mean open ocean influence as the only forcing. Experiment BC changes the sole open ocean forcing from the 10 year mean to daily to examine its time-varying influences. Experiments WS and HF add 6 hourly wind stress and heat flux, respectively, to the simplest experiment NO to examine their effects individually. The annual mean inflow/outflow used in experiments NO, WS, and HF is indicated around each open boundary of EAMS model in Figure 2. In the main channels on the southern boundary of EAMS, the transport values are compatible with observations. For example, *Wyrtki* [1961] proposed that the average Karimata Strait transport is about 0.7 Sv to the south. *Gordon et al.* [2008] suggested that the transport through the Makassar Strait is 11.6 Sv southward based on 3 year (2004–2006) mooring data.

[10] The four additional experiments do not start from a motionless state. Rather, they are continuation runs from the

Table 4. Summary of Numerical Experiments

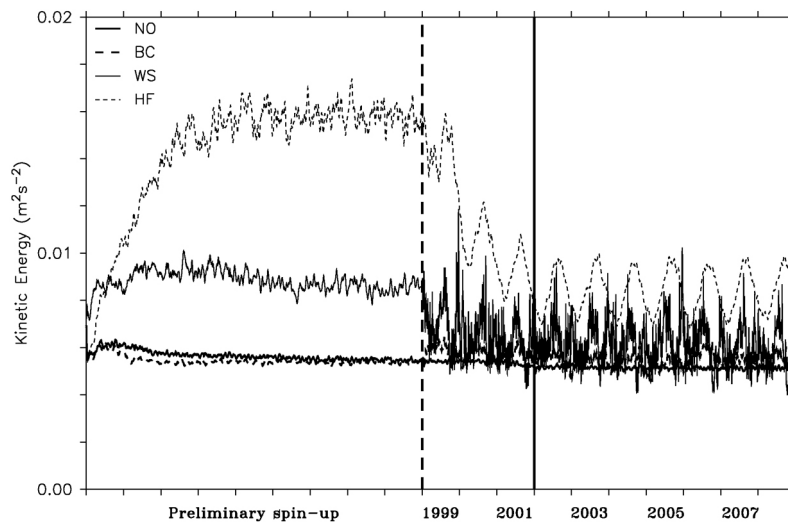| ID	Inflow/Outflow	Wind	Heat Flux
CTL	daily	6 hourly	6 hourly
NO	10 year mean	zero	zero
BC	daily	zero	zero
WS	10 year mean	6 hourly	zero
HF	10 year mean	zero	6 hourly

Figure 3. Domain-averaged kinetic energy for experiments NO, BC, WS, and HF. Dashed and solid vertical lines mark the beginning of 1999 and 2002, respectively.

all-inclusive EAMS model. If we eliminate certain types of forcing suddenly from the all-inclusive model and continue the simulation, undesirable transients will be triggered and could last for years. To avoid undesirable transients and ensure smooth transition require precautions, we invoke a two-step process to ease the transition. The aim of the first step is to remove selected forcing without triggering long-lasting adjustment-induced disturbances. While reducing the types of forcing, the remaining forcing is fixed at the strength on 1 January 1999 for 9 years to complete the preliminary spin-up. Thereafter, we resume the simulation with the remaining forcing having intended temporal resolutions from the beginning of 1999 to the end of 2008. The two-step process ensures smooth transition to a new statistical equilibrium state for each experiment. Leaving details of each experiment aside for later discussion, Figure 3 illustrates the smooth transition in terms of kinetic energy averaged over the entire model domain. The first-step adjustment brings each experiment to a new equilibrium in about 5 years. After adding time dependency from the beginning of 1999 (dashed vertical line), the average kinetic energy in all cases reaches an equilibrium level after 2002 (solid vertical line). We use results from 2002 to 2008 for later discussions.

3. Results

3.1. Mean Surface Circulation Around Luzon Strait

[11] Averaging from 2002 to 2008, Figure 4a shows the mean circulation at 100 m depth. A Kuroshio meander stands out, intruding into the SCS mostly via the Ballintang channel. The whole Kuroshio does not meander into the SCS; a portion stays outside the north-south running island chain that dots the Luzon Strait. Entering the Luzon Strait, the Kuroshio intrusion current shows visible bifurcation when and after it passes the northernmost end of Babuyan Islands (122°E, 19.5°N). Exiting the SCS, the Kuroshio meander rejoins the outer branch off southeast Taiwan. This flow pattern shows up in quite a few high-resolution models. These models differ in spatial discretization method, time stepping method, and underlying assumption in physics.

Despite differences, the overall flow pattern seems to transcend computation specifics among these models as long as they have adequate resolution to resolve the complex bathymetry [e.g., *Metzger and Hurlburt*, 2001a]. Further, long-term averaged observations across the Luzon Strait, from either surface drifters [*Centurioni et al.*, 2004] or shipboard ADCPs [*Liang et al.*, 2003], confirmed the existence of Kuroshio meander.

[12] The corresponding temperature field at 100 m depth tells more. The Kuroshio meander carries warm waters from the western Pacific into the SCS, delineated by 21°C contour in Figure 4b. There are also three distinct cold anomalies. The one west of the Luzon Island is the most expansive, ranging down to 7°C relative to surrounding waters. This corresponds to the cold West Luzon Eddy. A narrow cold band exists between the east coast of Taiwan and shoreward edge of the Kuroshio, commonly seen in NODC data and Ocean Data Bank of Taiwan. Though weakest among the three, another cold belt is seen southeast and east of the Hainan Island.

[13] Aside from mean circulation, variance reveals regional fluctuations from intraseasonal to seasonal. Figure 4c shows the root-mean-square (RMS) of modeled sea level anomaly after removing the mean sea level point by point over the 7 year period. A high-variance belt off southern China stands out, apparently in response to normally occurring, profound weather changes around weekly time scales in shallow water [*Zhuang et al.*, 2010]. Aside from shallow water, three high-variance regions (marked by A, B, and C) also stand out. Region A, west of the Luzon Strait, is well known for vigorous eddy shedding activities. Prior investigations have so far identified eddy shedding induced by the wax and wane of Kuroshio meander [e.g., *Wu and Chiang*, 2007] and fluctuating local wind stress curl [e.g., *Wu et al.*, 2005; *Hsin et al.*, 2010] as two sources of variability. Region B, off west Luzon, owes its high variability to the winter appearance (and summer disappearance) of the cold West Luzon Eddy [*Qu*, 2000]. Region C, southeast of the Hainan Island, also shows up in the variance map of *Metzger* [2003] and the standard deviation of sea
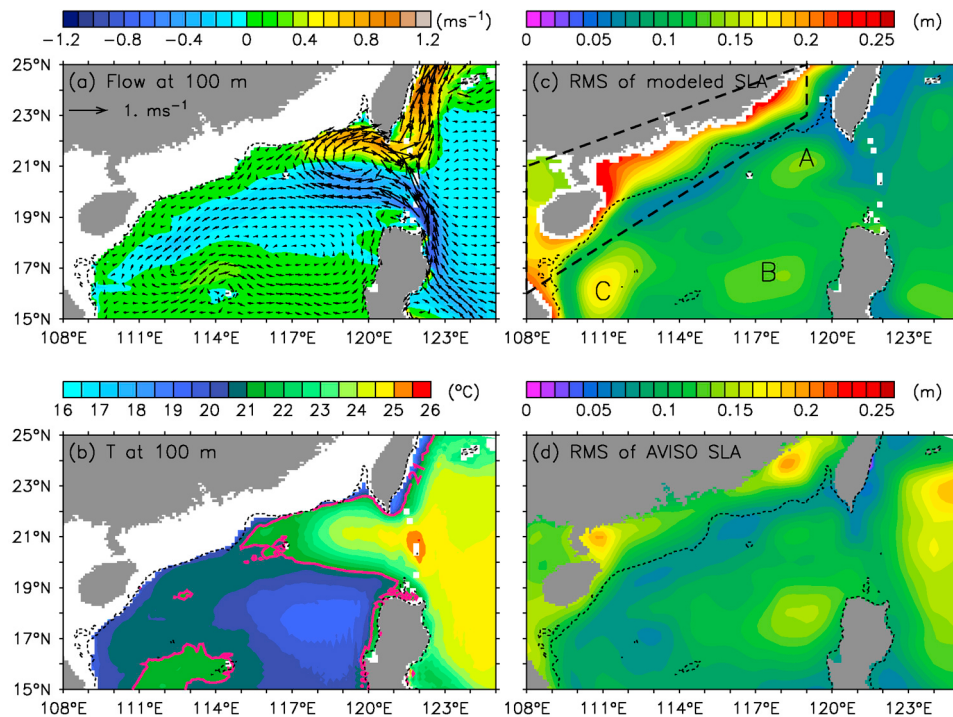
Figure 4. (a) Modeled 7 year mean flow (vector) at 100 m, color differentiated by the intensity of zonal velocity, (b) modeled temperature with 21°C isotherm in pink, (c) root-mean-square (RMS) of modeled sea level anomaly, and (d) RMS of satellite altimeter (AVISO) sea level anomaly. Thin dashed lines are 100 m isobath.

level variation of *Zhuang et al.* [2010]. *Zhuang et al.* [2010] suggested that the high intraseasonal variances west of the Luzon Strait (region A) and east of Vietnam (south of region C) are sources of variance southeast of the Hainan Island in winter and summer, respectively. Figure 4d shows corresponding 7 year (2002–2008) RMS derived from satellite altimeter sea level anomaly (AVISO; Archiving, Validation and Interpretation of Satellite Oceanographic data; http://www.aviso.oceanobs.com), lending support to our model (Figure 4c). Discrepancy does exist. For example, the RMS east of the Luzon Strait in model is lower than that in AVISO. The higher RMS east of Luzon Strait in AVISO is due to the ubiquity of mesoscale eddies in the subtropical countercurrent region (STCC) [*Qiu*, 1999]. The mismatch in the model field could be resulted from the poor simulation of eddies in the STCC region. Despite the mismatch, the model still catches the main features of SSH variance in the northern SCS.

3.2. Seasonal Variation

[14] Averaging over the 7 years (2002–2008) month by month, Figure 5 shows currents and temperature at 100 m for March, June, September, and December. The warm water intrusion waxes in fall and winter and wanes in spring and summer. In spring and summer (Figures 5a and 5b), the warm intrusion is pretty much confined within a well-rounded Kuroshio meander. In fall and winter (Figures 5c and 5d), however, the warm water intrudes farther into the SCS from the head of the Kuroshio meander. This intrusion is the farthest reaching in December (Figure 5d), extending to west of 112°E. It recedes thereafter to the east of 117°E in

June (Figure 5b). Hydrographic data analyses [*Shaw*, 1989, 1991; *Qu et al.*, 2000] lend further support; intrusive Pacific water can be found west of 117°E in winter but only east of 117°E in summer. In winter, some drifters can reach west of 112°E [*Centurioni et al.*, 2004, Figures 2 and 3d]. In addition, revealed in hydrographic data [*Shaw*, 1991, Figure 8], the Philippine Sea Water can be found in winter around 112°E. These results give further evidences for the far-reaching winter intrusion as shown in Figure 5d.

[15] Besides warm intrusion, the three cold anomalies also show seasonality. West of Luzon Island, the cold pool is maximal in December, virtually vanishes in July, and redevelops thereafter. Off east Taiwan, the cold water band, apparently as a result of upslope lifting of deeper water by the left-bounded Kuroshio, is much more significant in summer than in winter. Conceivably, downwelling-favorable monsoon wind in winter could suppress the upwelling to a degree. Off southern China, the cold water band appears only from May to September when the northeastward current is stronger. Again, upslope lifting of cold waters by the left-bounded current should be the cause.

3.3. Variability of Transports in the Luzon Strait

[16] The modeled mean LST along 120.75°E has a layered structure, with outflow from 20 to 150 m, inflow from 150 to 1200 m, outflow from 1200 to 2300 m, and little net transport below that (solid line in Figure 6a). A layered structure is also suggested by sparse observations (Table 3) but with varying layer boundaries. The 20–150 m net outflow in the model has not been observed to date. However, our 0–200 m modeled LST agrees very well with the AVISO-based
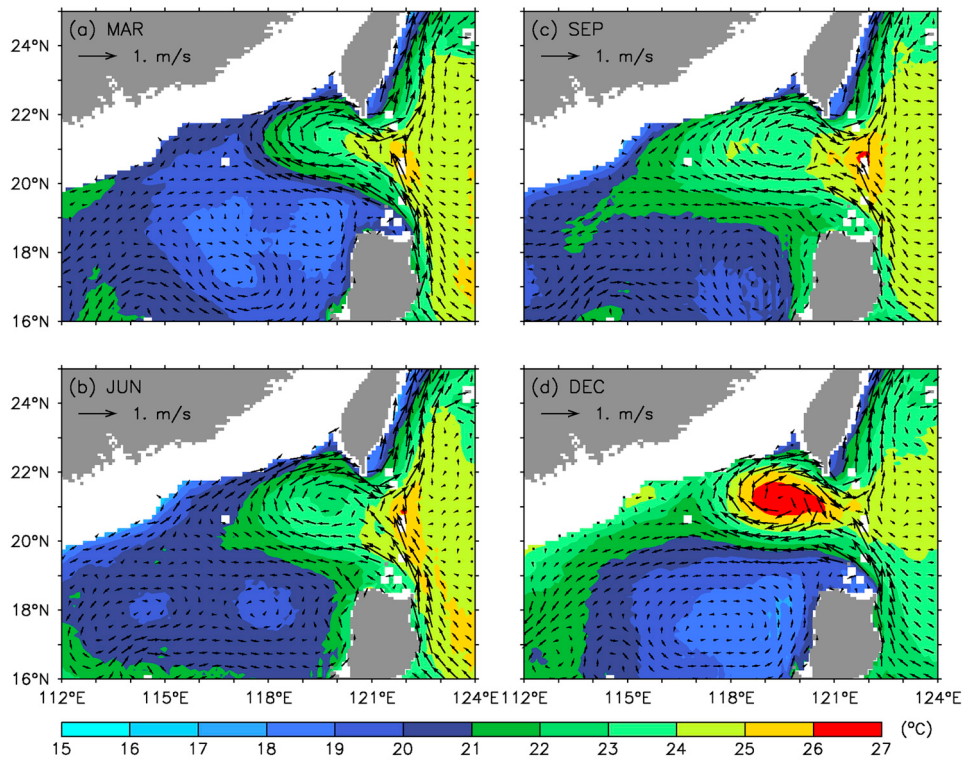
Figure 5. Modeled flow (vector) and temperature (color) at 100 m in (a) March, (b) June, (c) September, and (d) December.

geostrophic transport integrated form surface down to 200 m (not shown), indicating that this layer could be true. Nevertheless, there is no substitute for in situ measurements. Future measurements concerning this are very much desirable. Integrating over the full depth range, the modeled mean LST, -4.0 ± 5.1 Sv (Figure 6b), is within the range of previous estimates (Tables 1 and 2). It is the small difference between the much larger vertical integrals of westward (-41.5 ± 5.4 Sv) and eastward (37.5 ± 6.6 Sv) flow. The standard deviation of total transport per unit depth (dashed

line in Figure 6a) is highly surface intensified, so are the standard deviations of westward and eastward transport per unit depth (not shown).

[17] The net LST in the upper layer has a large westward transport in winter but is much weaker in summer [e.g., *Wyrtki*, 1961; *Shaw*, 1991; *Qu*, 2000]. Obviously, the upper layer transport varies somewhat with the depth scale chosen. Our choice of 600 m to represent upper layer of the Luzon Strait arises from our intention to better represent the warm layer intrusion into the SCS. When averaged over a year or
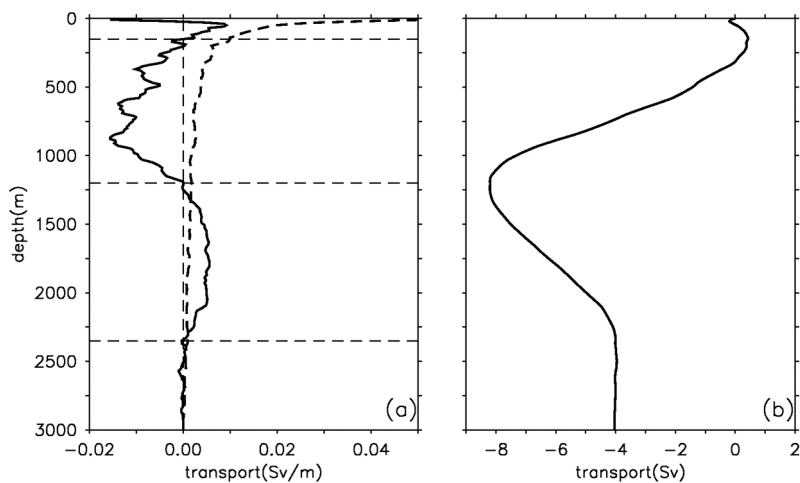

Figure 6. Depth-specific distributions of (a) mean Luzon Strait transport per unit depth (solid line) and corresponding standard deviation (dashed line) and (b) cumulative transport from the surface down.
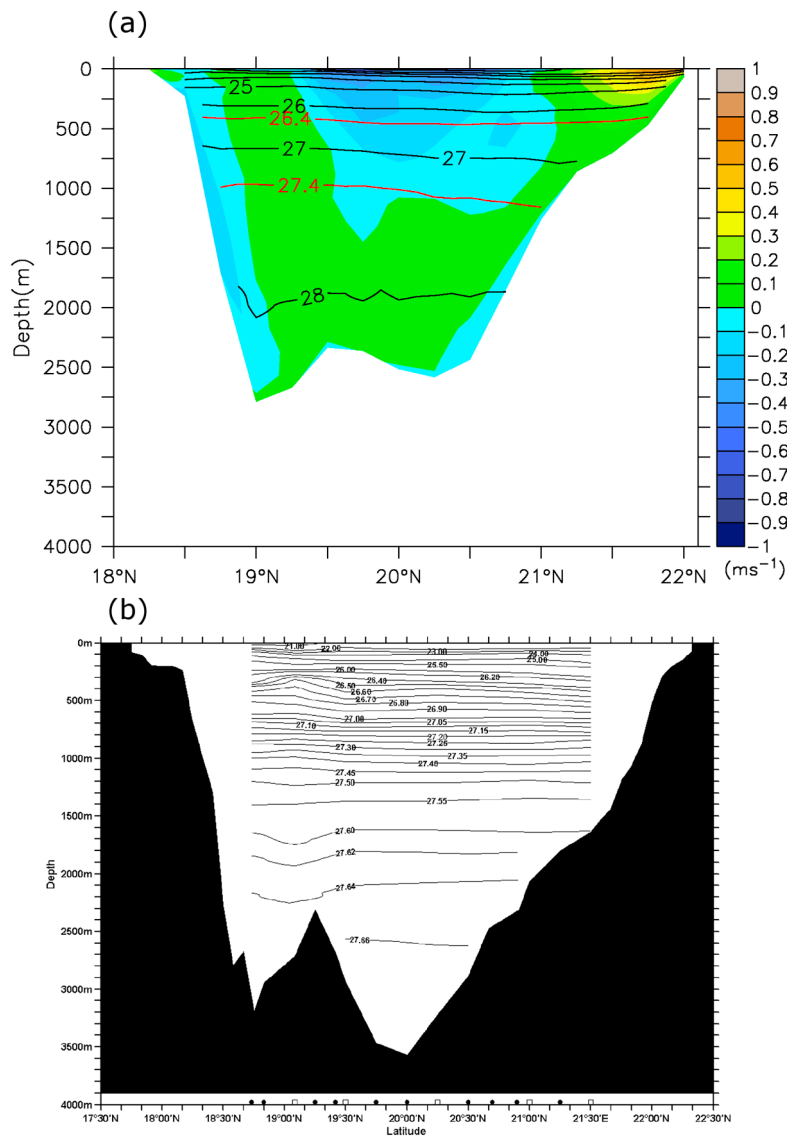
Figure 7. Vertical sections of (a) modeled mean zonal velocity (color shading) and potential density (contours in kg m^{-3}) along 120.75°E in October 2005 and (b) corresponding observed potential density during 4–16 October 2005 [*Tian et al.*, 2006].

multiple years, our model results suggest 600 m as the relevant depth scale for the warm water intrusion. Below 600 m, especially below 750 m, is the cold water intrusion, which has the opposite effect on the regional climate. Previous observation-based estimates lend further support. Figure 7a shows distributions of simulated zonal velocity and potential density across the Luzon Strait. The modeled potential density distribution agrees with the concurrent observation (Figure 7b) [from *Tian et al.*, 2006]. *Tian et al.* [2006] used 26.4 and 27.4 kg m^{-3} isopycnals, which represent the lower boundaries of the North Pacific Tropical Water (NPTW) and the North Pacific Intermediate Water (NPIW), respectively [*Qu et al.*, 1999], to delineate the upper, middle, and lower layers in the Luzon Strait. The corresponding depths, roughly at 500 and 1000 m, are consistent with the optimum estimates from our model. In fact, upper ocean LST (UpLST) varies little whether we use 600 m (solid lines in Figure 8) or 26.4 kg m^{-3} isopycnal

(dashed lines in Figure 8) as the reference depth. Both estimates agree in magnitudes and seasonality. According to Figure 6a, the depth of 1200 m (the zero-crossing point) could be another choice of calculating UpLST. We regard the transport above 1200 m as the maximum UpLST, but it does not better represent the warm layer intrusion into the SCS. Nevertheless, the transport above 1200 m has the same seasonality with the transports above 600 m and above 26.4 kg m^{-3} isopycnal with a larger mean westward transport (not shown). Weighing all the issues above, we therefore use 600 m depth, roughly the depth of upper ocean inflow and outflow, to represent UpLST. *Tian et al.* [2006] and *Yang et al.* [2010] chose the reference depth in a similar way.

[18] In the upper 600 m of our model (Figure 8a), the net UpLST peaks to 2.7 Sv (eastward) in June and −8.4 Sv (westward) in December. Corresponding UpLST estimate by *Qu* [2000] using hydrographic data is about −3.0 Sv
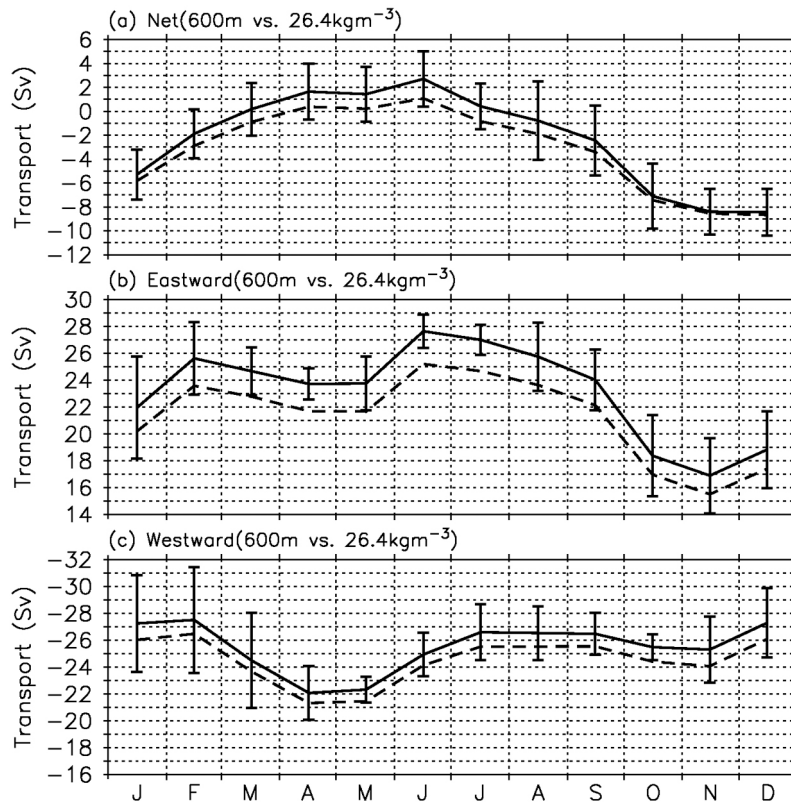
Figure 8. Monthly Luzon Strait transport derived from the EAMS model, averaged from 2002 to 2008: (a) top 600 m net, (b) top 600 m eastward, and (c) top 600 m westward. The dashed lines are corresponding transports above the potential density surface of 26.4 kg m^{-3}. Vertical bars are standard deviations.

when averaged over a year, peaking to −5.3 Sv in January–February and bottoming out to −0.2 Sv in June–July. Quantitative discrepancies aside, Qu's estimate shows similar seasonal cycle. Monthly variance of UpLST (vertical bars) is sizable (2.7–3.3 Sv) in August–October and smaller (about 2 Sv) in the rest months. The December minimum variance presumably indicates the stability of the Kuroshio meander when it has developed to the fullest, while large variances from August to October arise from surging interannual variability. Figures 8b and 8c show monthly UpLST of eastward outflow and westward inflow. The eastward only UpLST (or outflow) levels off at about 25 Sv between February and May, peaks in June, and bottoms out in November. The westward only UpLST (or inflow) is maximal from December to January, when the Kuroshio east of the Luzon Island is the weakest, and minimum in April, when the monsoon changes from northeast to southwest. Interestingly, April is also when the Kuroshio is the strongest east of the Luzon Island [*Qiu and Lukas*, 1996]. There is also a barely visible, secondary minimum in November, when the monsoon changes from southwest to northeast (Figure 8c).

[19] Variance-preserving spectra after the fast Fourier transform reveal more. Figures 9a, 9b, and 9c show the spectra of the net, eastward only, and westward only UpLSTs, respectively. For the net UpLST, peaks at 365, 180, 130, 90–100, 70, and 40–60 days stand out, of which the first two are annual and semiannual. Almost all

oscillations remain intact in eastward only and westward only UpLSTs, except for the much weakened 130 day oscillations in westward only UpLST. East of the Luzon Island, most of these oscillations in the Kuroshio region also survive with varying degree of intensity (results not shown). For example, the annual signal no longer stands out as much, being partially masked by westward propagating mesoscale eddies from the interior Pacific with dominant periods from 100 to 130 days [e.g., *Johns et al.*, 2001].

4. Other Numerical Experiments

[20] As listed in Table 4, we discuss four additional experiments below to identify the relative importance of open ocean boundary forcing, regional wind stress, and surface heat fluxes on the variation of UpLST.

4.1. Steady Inflow and Outflow Only: Case NO

[21] Experiment NO eliminates wind stress and surface heat fluxes while fixing the open ocean inflows/outflows at the 10 year mean from NPO model. Averaging from 2002 to 2008, Figure 10 shows essential results after the maximum simplification. The UpLST (Figure 10a) becomes almost a constant eastward outflow from the SCS, about 4 Sv throughout. The fact indicates that a steady Kuroshio, which is built up from a steady inflow/outflow (NEC/downstream Kuroshio) along the southern/northern part of eastern boundary, can set up a steady outflow of UpLST up to 4 Sv.
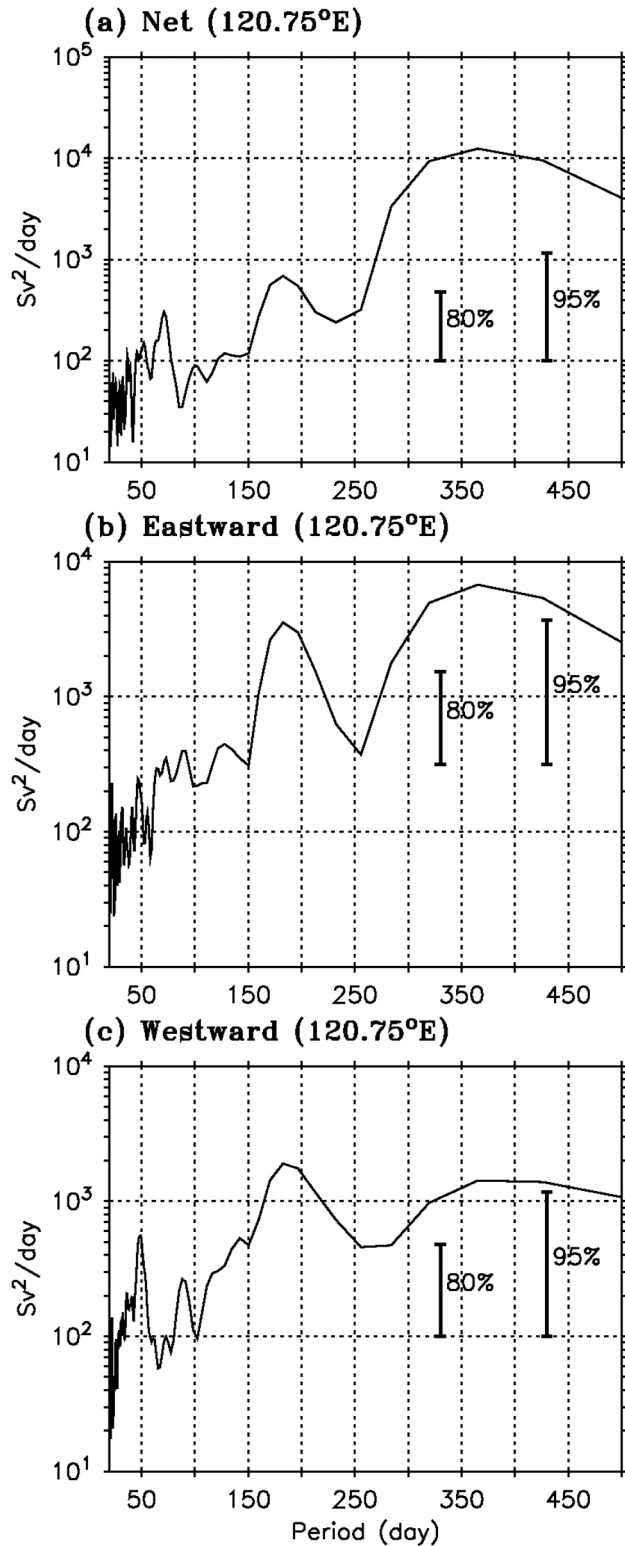
(a) Net (120.75°E)

(b) Eastward (120.75°E)

(c) Westward (120.75°E)

Figure 9. Variance-preserving spectra of top 600 m transports along 120.75°E: (a) net, (b) eastward only, and (c) westward only. Vertical bars are 80% and 95% confidence intervals.

The flow (Figures 10c and 10d) and the temperature at 100 m (Figures 10e and 10f) show no monthly variation as expected. The annual signal also disappears from UpLST spectrum (Figure 10b) as anticipated. Aside from steadiness, some intraseasonal oscillations (most notably from 40 to 60 days) still persist in Figure 10b.

4.2. Daily Inflows and Outflows Only: Case BC

[22] Changing inflows and outflows from the 10 year mean to daily (and excluding winds and surface heat fluxes as in case NO), experiment BC begins to recover some of the annual cycle of UpLST as seen from the monthly climatology (Figures 11a and 11b). Nevertheless, the average UpLST over a year cycle (black solid line) does not deviate much from that in experiment NO. Unlike the all-inclusive control run (red line), the monthly maximum and minimum of the UpLST occur in April and November, respectively. Subtracting the 10 year mean outflow (experiment NO) from daily fluctuations (experiment BC), the remnant UpLST from demeaned daily fluctuations alone (dashed line) indicates eastward outflow of UpLST in March–July by as much as 2 Sv in April–May and westward inflow in other months ranging up to −2 Sv in October–December. Observationally, the northward Kuroshio transport east of the Luzon Island is maximum in March–April and minimum in September–October [*Qiu and Lukas*, 1996]. Our westward only UpLST from the control run (Figure 8c) also reaches minimum in April. Combining their observation with our modeling exercise (and from a mass balance point of view), a larger northward Kuroshio transport off east Luzon seems to occur at the expense of inflow (westward only UpLST) to the SCS. *Sheremet* [2001], on the basis of an idealized model simulation, also concluded that a stronger western boundary current tends to follow a straight path rather than meandering into a gap. Our model behaves similarly and shows reduced westward inflow in April. In addition to the annual signal, peaks around 50 and 180 days are also present in Figure 11b.

[23] Figures 11c–11f show currents and temperatures at 100 m for April and November; the eastward UpLST becomes maximal and minimal, respectively. Visually, the flow and temperature patterns in the northern SCS do not differ much between the 2 months. When the outflow is minimal in November, the intrusive Kuroshio meander current west of 117°E intensifies slightly. Relative to April, the November temperature is slightly warmer inside the Kuroshio meander but slightly colder south of it. The shore-parallel current off southern China is similar between the 2 months with a slightly weaker northeastward velocity in November, indicating its insensitivity to open ocean forcing.

4.3. Wind Forcing: Case WS

[24] Adding 6 hourly winds to the steady open ocean forcing case (experiment NO), winds emerge as the major force driving the UpLST in case WS (black solid line in Figure 12a). Subtracting the corresponding UpLST of case NO from it, the dashed line in Figure 12a singles out the wind effect alone. Being an inflow throughout a year cycle (except for a little outflow in June), the wind-alone UpLST (dashed line) contains almost the same seasonality as in the all-inclusive experiment CTL (red line) with maximum in December and minimum in June.
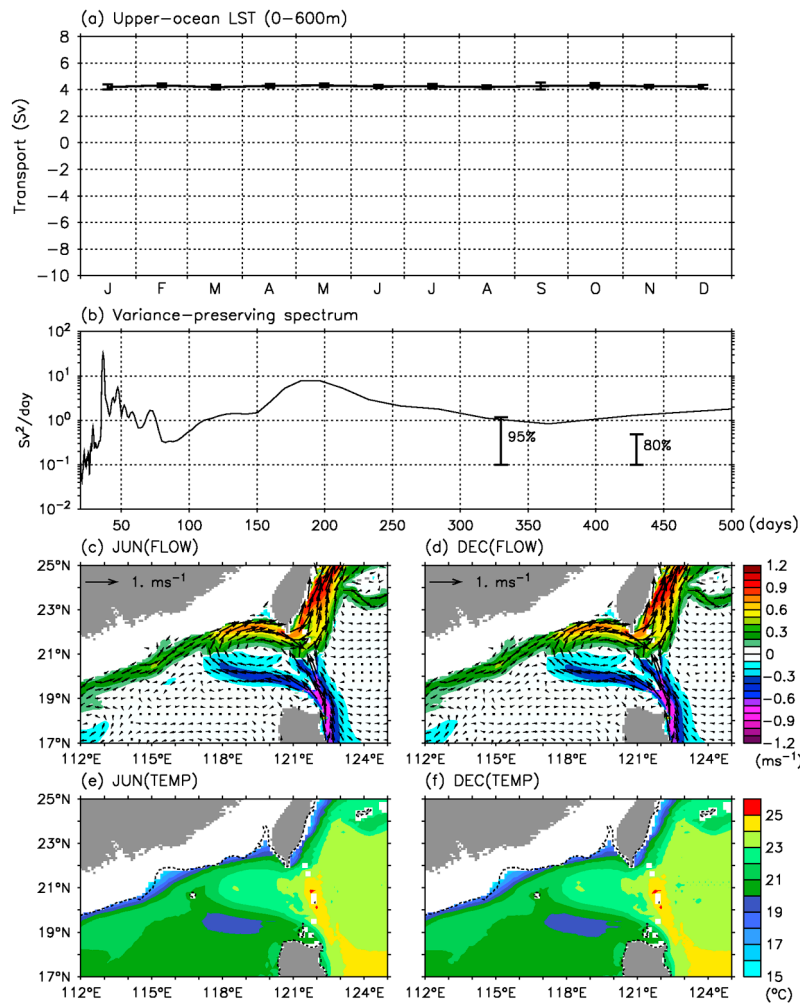
Figure 10. Results from experiment NO after averaging from 2002 to 2008: (a) monthly UpLST, (b) variance-preserving spectrum of the UpLST with 95% and 80% confidence intervals. Flow pattern at 100 m in (c) June and (d) December. Temperature field at 100 m in (e) June and (f) December. Currents are color-differentiated according to the intensity of zonal velocity. Dashed lines in Figures 10e and 10f are 100 m isobath.

[25] Since the seasonal monsoon reversal is back, the annual signal also returns to the variance-preserving spectrum (Figure 12b). Below annual cycle, peaks around 40–60 days also return. Seasonal changes of circulation and temperature at 100 m become much more pronounced (Figures 12c–12f). In December, for example, the Kuroshio intrusion regains its vigor to radiate warm intrusion ahead of the well-rounded meander head to west of 117°E (Figures 12d and 12f). Also recovered is the seasonality of a northeastward current (the so-called South China Sea Warm Current) over the continental shelf off southern China. It spans the entire shore-parallel distance from west of 112°E to the southern Taiwan in June (Figure 12c), but the northeast monsoon in December is able to stop most of it (Figure 12d). The mean winter condition does not tell the whole story. On weekly time scales, however, a recent modeling study [*Chiang et al.*, 2008] ties occasional winter appearances of the South China Sea Warm Current to wind relaxation events. The two shore-parallel bands of cold water, one off southern China and the other off east coast of Taiwan, also regain proper seasonality. As in the all-inclusive experiment CTL, the former disappears while the latter weakens in December.

4.4. Surface Heat Flux: Case HF

[26] Previous LST estimates tie their variations to either local versus remote wind stress or northward Kuroshio transport off east Luzon [e.g., *Metzger and Hurlburt*, 1996; *Qu*, 2000; *Sheremet*, 2001; *Liang et al.*, 2008]. Little is known about the effect of the surface heat flux. Borrowing similar analysis from the region off northeast Taiwan [*Oey et al.*, 2010], the effect of heat flux appears to be non-negligible. Winter cooling in that region induces downslope movement of dense shelf water, causing a shoreward shift of the Kuroshio to fill part of the void. Moving from case WS to case HF, we replace wind forcing by surface heat flux to examine its effect.

[27] The combination of 6 hourly heat flux and steady open ocean inflow/outflow generates a seasonally varying
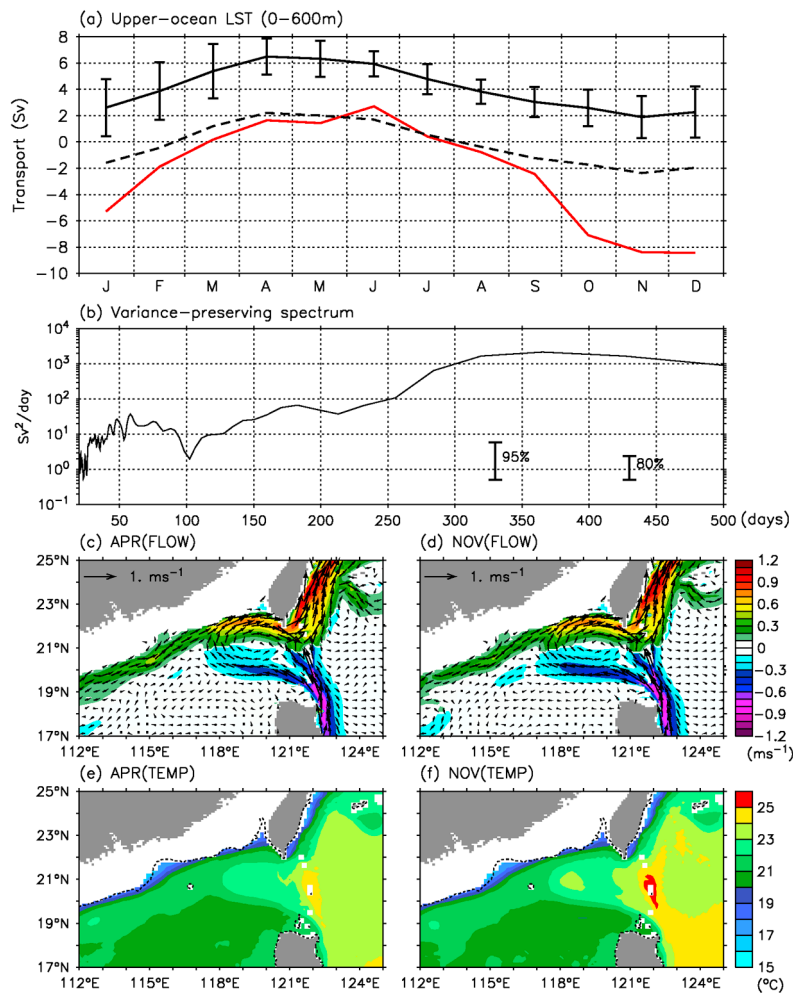
Figure 11. Results from experiment BC after averaging from 2002 to 2008: (a) monthly UpLST (solid black line), remnant of UpLST after subtracting experiment NO from it (dashed black line) and reference UpLST from the all-inclusive experiment CTL (red line); (b) variance-preserving spectrum of the UpLST. Flow pattern at 100 m in (c) April and (d) November. Temperature field at 100 m in (e) April and (f) November.

UpLST outflow (black solid line in Figure 13a). However, its phase deviates considerably from preceding cases, having minimum in February and maximum in August. After removing open ocean forcing (experiment NO) from UpLST, the heat flux alone leads to westward inflow all year round (dashed line). Annual and semiannual signals are conspicuous in the variance-preserving spectrum (Figure 13b), and so are oscillations of 40–60 days. Currents at 100 m show a southwestward intrusive current from east of the Luzon Strait, radiating far into the SCS. Bordered to its north is a northeastward shelf current off southern China, exiting the Luzon Strait eventually (Figures 13c and 13d). The two currents vary little seasonally. The UpLST inflow induced by heat flux alone is minimal in August. Temperature also varies little seasonally (Figures 13e and 13f).

5. Discussion and Conclusions

[28] This paper uses an observation-validated, three-dimensional model to facilitate an updated, in-depth examination of Luzon Strait transport and circulation around it.

Entering the SCS, the intruding Kuroshio meander waxes in winter but wanes in summer, leading to an annual mean, westward LST (-4.0 ± 5.1 Sv) along 120.75°E. Past estimates from models and data suggested a three-layered LST, having two inflows in upper and lower depths separated by a middepth outflow. With improved grid resolution in modeling and temporal resolution in forcing, we suggest the emergence of an additional layer (shallow outflow) between 20 and 150 m. However, when partitioning layer thicknesses more or less in line with the past conventions, the long-believed three layers reemerge.

[29] We have also assessed the relative importance of open ocean inflow/outflow, wind stress, and surface heat flux in driving LST in the top 600 m. The process of elimination singles out the wind stress as the dominant forcing for it alone can produce the right seasonality of Kuroshio intrusion and UpLST. The open ocean inflow/outflow, whether steady or daily, induces an eastward outflow rather than a commonly believed inflow, not to mention the distorted seasonal variation. The heat flux alone can also force a westward inflow of UpLST, but with misaligned seasonality.
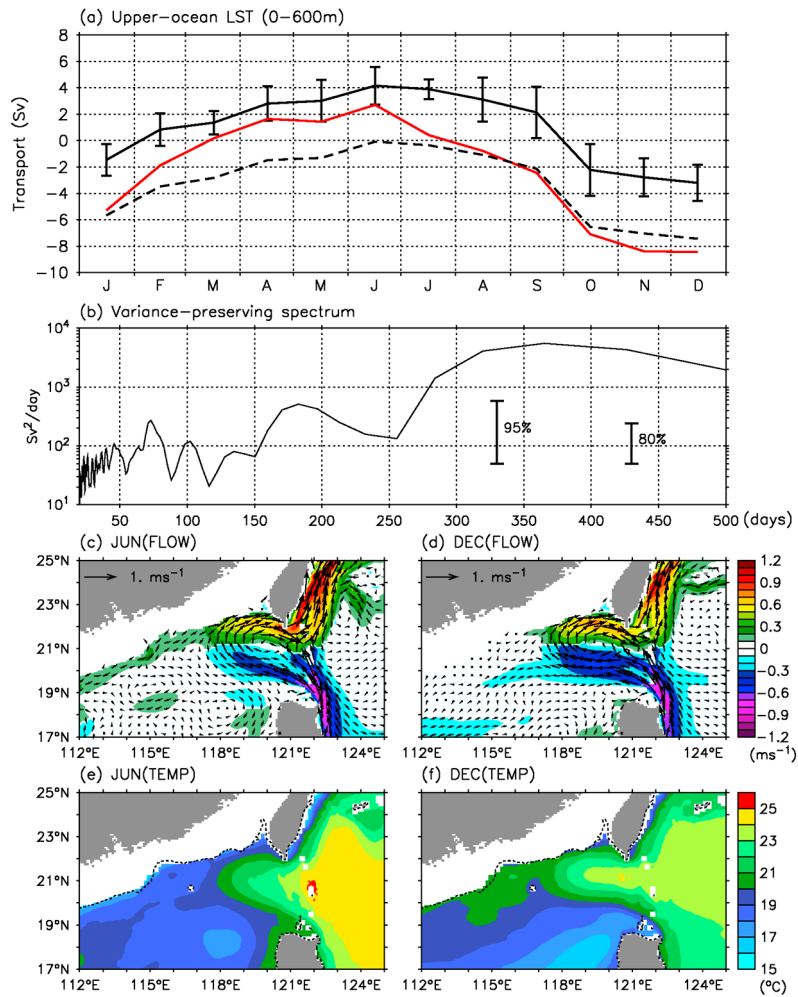
Figure 12. Same as Figure 11 but for experiment WS and with a change of selected months to June and December in Figures 12c–12f.
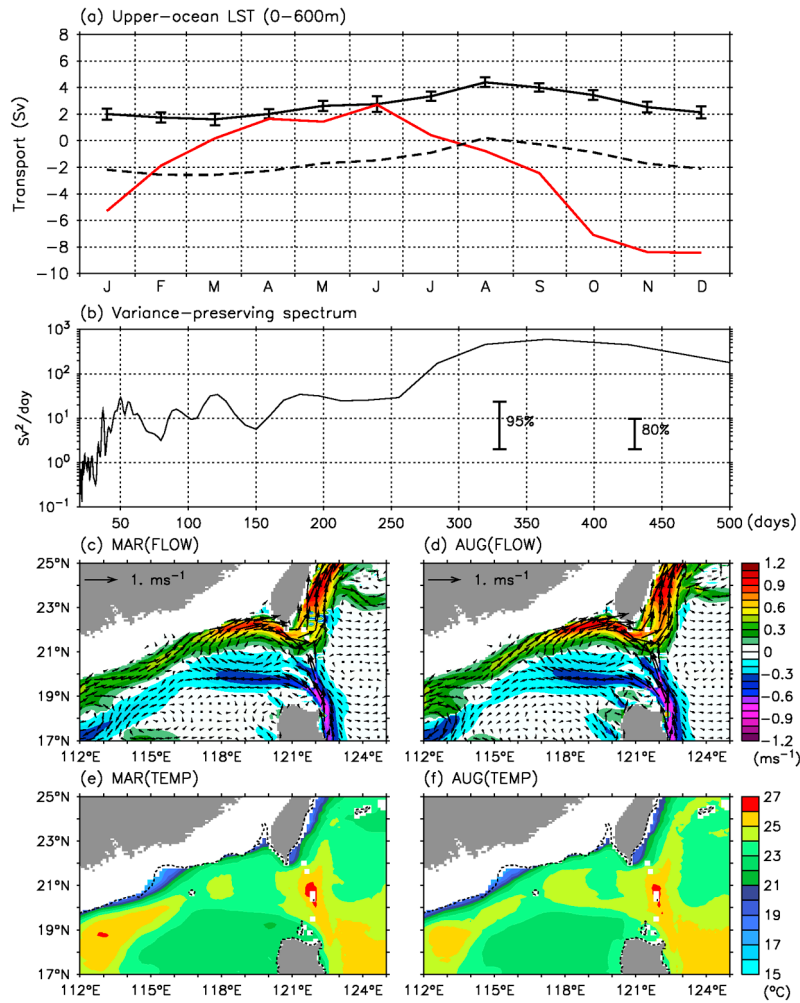
Figure 13. Same as Figure 11 but for experiment HF and with a change of selected months to March and August in Figures 13c–13f.
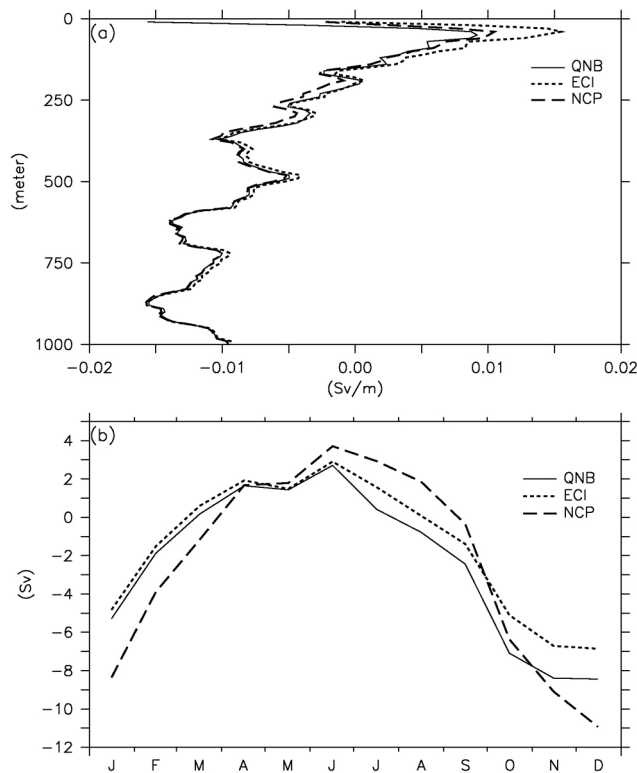
Figure 14. (a) Depth-explicit distributions of mean LSTs over the period from 2002 to 2008 with QuikSCAT/NCEP blended wind (QNB), ECMWF Interim reanalysis wind (ECI), and NCEP reanalysis wind (NCP). Averaging month-by-month instead from 2002 to 2008. (b) The corresponding monthly distribution of UpLST (above 600 m).

[30] *Metzger* [2003] uses a $1/16° \times 1/16°$ Naval Research Laboratory Layered Ocean model to examine the sensitivity of the SCS circulation to different monthly wind field and monthly wind stress curl. As he sees it, the generation of West Luzon Eddy is controlled by the wind stress curl. But the degree of Kuroshio intrusion into the Luzon Strait is not. Extending the monthly climatology to higher-frequency wind products, our model also shows low sensitivity of the Kuroshio intrusion to winds. Figure 14 compares the skill level of three wind products in producing the Luzon Strait transport: QuikSCAT/NCEP blended winds, $1.5° \times 1.5°$ ECMWF Interim Reanalysis (http://data-portal.ecmwf.int/) and $2.5° \times 2.5°$ NCEP Reanalysis. All three wind products are implemented in the same way as described in the control run and lead to similar results except with minor variations. When integrated north-south across the channel, all three show similar inflow/outflow profiles (Figure 14a), except the ECMWF wind generates the largest eastward outflow in the top 100 m. Further, all three monthly UpLSTs show maximum outflow in June and maximum inflow in December (Figure 14b).

[31] The UpLST arises mostly from westward intrusion of the Kuroshio meander from the Luzon Strait to the northern SCS. Previously suggested mechanisms regulating its strength are many, including the meridional pressure gradient across the Luzon Strait [*Qu*, 2000], local wind stress curl

inside SCS [*Liang et al.*, 2008], seasonal variation of monsoon winds [*Metzger and Hurlburt*, 1996], and the Pacific basin-scale wind field changes [*Zhao et al.*, 2009]. They may be all related because changes in one factor affect others. In our view, it may be futile to choose the winner among all factors. Beyond previously suggested mechanisms, local baroclinic instability of the Kuroshio may also be a suspect regulating the strength of UpLST. Following the last lead raised during the review process, we have enhanced or weakened the wind stress of the control run twofold to check whether the changes will preferentially alter the mean or the standard deviation of UpLST. The results, briefly illustrated in Figure 15 and presented in Table 5, show no lopsided sensitivity; both the mean and standard deviation of UpLST increase or decrease with wind strength changes profoundly. This conclusion, combined with our analysis of Figure 17 and Table 5, points to the monsoon wind as the dominant driving mechanism regulating the strength of UpLST. Nevertheless, we should put our finding in the larger perspective that all previously suggested mechanisms may be interrelated, and it is difficult to choose a winning one over others.

[32] The previously undocumented and yet to be confirmed layer (roughly between 20 and 150 m as mentioned in section 3.3) of mean eastward transport in the Luzon Strait requires discussion. This layer persists even in the absence of wind, surface heat flux, and seasonal variation of the Kuroshio (in experiment NO). As shown in Figure 16, the eastward transport in experiment NO (thick solid line) is a surface intensified feature extending to about 350 m deep. If we include wind and heat flux (in experiment CTL), only the transport above 20 m becomes westward, apparently caused by the westward Ekman drift associated with the prevailing northeasterly wind in winter. The transport below 20 m is still eastward (against the Ekman transport) because of the strong mean eastward transport. Furthermore, Figure 15a also shows the sensitivity of mean LST in the 20–150 m layer to wind strength. Doubling the wind stress will change the LST in this layer from eastward to westward, while reducing wind stress twofold will enhance the eastward LST in this layer. The contribution of these changes comes mainly in winter.

[33] In the studies by *Metzger and Hurlburt* [2001a] and *Metzger* [2003], the Kuroshio intrusion in the Luzon Strait is sensitive to the model's ability to resolve the Luzon Strait island chain. These islands are better defined with enhanced model resolution. In particular, the Kuroshio intrusion decreases markedly when their model's ability to resolve the island chain increases from $1/2°$ (as in the study by *Metzger and Hurlburt* [2001a]) to higher than $1/16°$ (as in the study by *Metzger* [2003]). Our model, on the other hand, does not show similar sensitivity if the resolution increases from $1/8°$ (the present model) to $1/16°$ [*Wu and Chiang*, 2007, Figure 8] because of our added precaution to restore the island chain every time we change the model resolution.

[34] As listed in Table 5, removing wind stress invariably triggers a sizable eastward outflow of UpLST despite the presence of other forcing. This requires explanation. We do so by examining the water mass exchange of the SCS with surrounding seas through five major pathways: the Luzon Strait (LS), Taiwan Strait (TWS), Mindoro Strait (MDS), Balabac Strait (BBS), and Karimata Strait (KMS) in Figure 17. Except for Luzon Strait, the Mindoro Strait is also deep
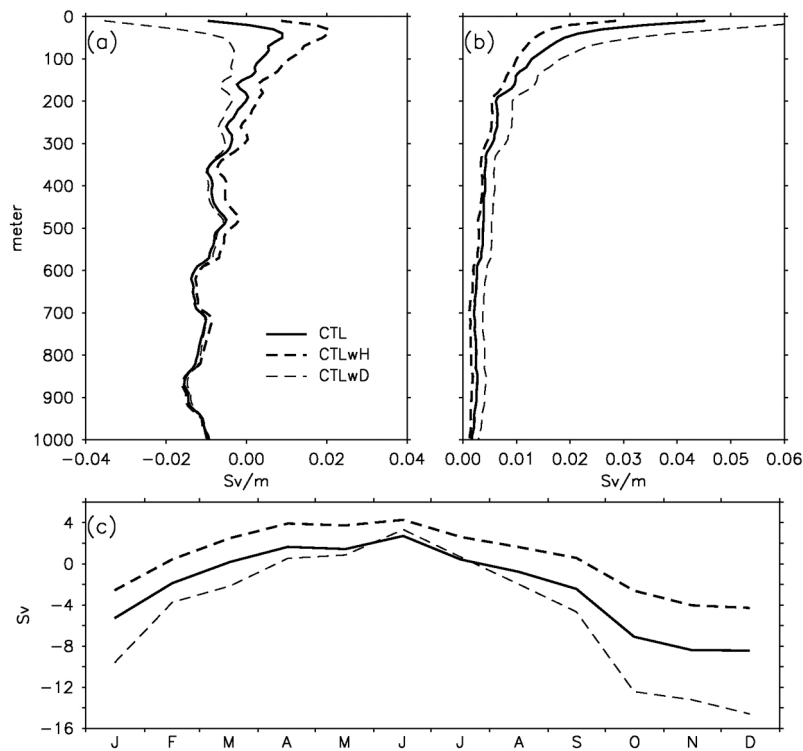
Figure 15. Depth-explicit distributions of (a) mean LSTs and (b) their standard deviations averaged over the period from 2002 to 2008 for the control run with full wind stress (CTL in solid line), halved wind stress (thick dashed line, CTLwH) and doubled wind stress (thin dashed line, CTLwD). (c) The corresponding monthly distribution of UpLSTs (above 600 m) but averaging month-by-month instead from 2002 to 2008.

(but narrow). Other straits are generally shallow. Figure 17b shows top 600 m transports through the five straits from all five numerical experiments. In the all-inclusive run (CTL), the westward Luzon Strait inflow exits the SCS through the Taiwan Strait, Karimata Strait and Mindoro Strait. Removing the wind stress reverses the Luzon Strait transport from an inflow to an outflow of up to 4 Sv. In compensation, an inflow of varying strength rushes into the SCS from the Sulu Sea through the Mindoro Strait.

[35] Briefly stated, the transport through Mindoro Strait is dictated by the sea level difference between the SCS and Sulu Sea. Discounting monsoon winds, sea level in the Sulu Sea should be generally higher because it receives the Indonesian Throughflow before the SCS. This factor alone invites an inflow from the Sulu Sea to the SCS (and, consequently, outflow through the Luzon Strait). On the other

Table 5. Mean and Standard Deviations of Upper Ocean Luzon Strait Transports From the Five Model Experiments[a]

| | Model Experiments | | | | | | |
Case	CTL	NO	BC	WS	HF	DW[b]	HW[c]
Mean	−2.3	4.3	4.1	0.9	2.7	−4.7	0.5
SD	5.0	0.3	2.3	3.5	1.1	7.8	3.8

[a]Transport in Sv. DW and HW are deviations from the control run (CTL) if the wind stress is enhanced or decreased twofold. Transports are averaged over the period from 2002 to 2008.
[b]Control run with doubled wind stress.
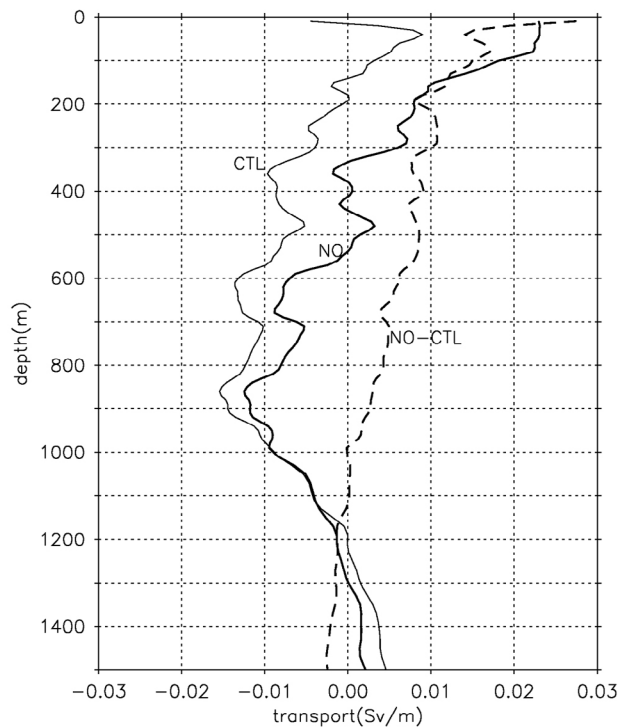[c]Control run with halved wind stress.

Figure 16. Depth-specific distributions of mean Luzon Strait transport per unit depth derived from experiments CTL (thin line) and NO (thick line). Dashed line depicts the transport difference between experiments NO and CTL.
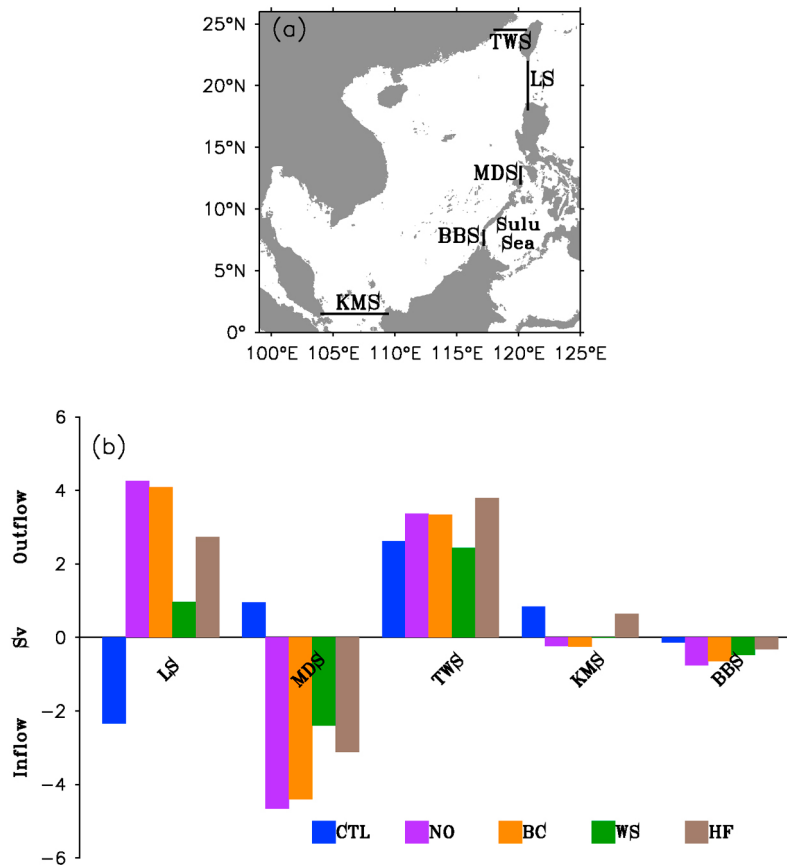
Figure 17. (a) Locations of Luzon Strait (LS), Mindoro Strait (MDS), Taiwan Strait (TWS), Karimata Strait (KMS) and Balabac Strait (BBS). (b) Upper ocean transports (above 600 m) through the five straits from the five experiments listed in Table 4. Inflow to and outflow from the SCS are negative and positive, respectively.

hand, the monsoon winds over the SCS, when averaged over a year, are decisively from the northeast because of the domination of winter winds. The northeast wind moves waters southward, raising sea level in the middle and southern reaches of the SCS to slightly above the Sulu Sea. Thus, the mean wind invites outflow from the SCS to the Sulu Sea (or inflow from the Luzon Strait). Weighing the two competing factors together, we see the cessation of northeast monsoon as a condition favorable for the Luzon Strait outflow or the Mindoro Strait inflow. While this mechanism works on and beyond annual time scale, its validity down to event-like time scales remains to be verified.

References

Centurioni, L. R., P. P. Niller, and D.-K. Lee (2004), Observations of inflow of Philippine Sea surface water into the South China Sea through the Luzon Strait, *J. Phys. Oceanogr.*, *34*, 113–121, doi:10.1175/1520-0485(2004)034<0113:OOIOPS>2.0.CO;2.

Chen, C.-T. A., and M. H. Huang (1996), A mid-depth front separating the South China Sea water and the Philippine Sea water, *J. Oceanogr.*, *52*, 17–25, doi:10.1007/BF02236530.

Chiang, T.-L., C.-R. Wu, and S.-Y. Chao (2008), Physical and geographical origins of the South China Sea Warm Current, *J. Geophys. Res.*, *113*, C08028, doi:10.1029/2008JC004794.

Chu, P. C. (1995), P-vector method for determining absolute velocity from hydrographic data, *Mar. Technol. Soc. J.*, *29*(3), 3–14.

Chu, P. C., and R. Li (2000), South China Sea isopycnal-surface circulation, *J. Phys. Oceanogr.*, *30*, 2419–2438, doi:10.1175/1520-0485(2000)030<2419:SCSISC>2.0.CO;2.

Fang, G., D. Susanto, I. Soesilo, Q. Zheng, F. Qiao, and Z. Wei (2005), A note on the South China Sea shallow interocean circulation, *Adv. Atmos. Sci.*, *22*, 946–954, doi:10.1007/BF02918693.

Gordon, A. L., R. D. Susanto, A. Ffield, B. A. Huber, W. Pranowo, and S. Wirasantosa (2008), Makassar Strait throughflow, 2004 to 2006, *Geophys. Res. Lett.*, *35*, L24605, doi:10.1029/2008GL036372.

Hsin, Y.-C., C.-R. Wu, and P.-T. Shaw (2008), Spatial and temporal variations of the Kuroshio east of Taiwan, 1982–2005: A numerical study, *J. Geophys. Res.*, *113*, C04002, doi:10.1029/2007JC004485.

Hsin, Y.-C., T. Qu, and C.-R. Wu (2010), Intra-seasonal variation of the Kuroshio southeast of Taiwan and its possible forcing mechanism, *Ocean Dyn.*, *60*, 1293–1306, doi:10.1007/s10236-010-0294-2.

Johns, W. E., T. N. Lee, D. Zhang, R. Zantopp, C.-T. Liu, and Y. Yang (2001), The Kuroshio east of Taiwan: Moored transport observations from the WOCE PCM-1 array, *J. Phys. Oceanogr.*, *31*, 1031–1053, doi:10.1175/1520-0485(2001)031<1031:TKEOTM>2.0.CO;2.

Lan, J., X. Bao, and G. Gao (2004), Optimal estimation of zonal velocity and transport through Luzon Strait using variational data assimilation technique, *Chin. J. Oceanology Limnol.*, *22*, 335–339, doi:10.1007/BF02843626.

Lebedev, K. V., and M. I. Yaremchuk (2000), A diagnostic study of the Indonesian Throughflow, *J. Geophys. Res.*, *105*, 11,243–11,258, doi:10.1029/2000JC900015.

Levitus, S., and T. P. Boyer (1994), *World Ocean Atlas 1994*, vol. 4, *Temperature*, *NOAA Atlas NESDIS*, vol. 4, 129 pp., NOAA, Silver Spring, Md.

Levitus, S., R. Burgett, and T. P. Boyer (1994), *World Ocean Atlas 1994*, vol. 3, *Salinity*, *NOAA Atlas NESDIS*, vol. 3, 111 pp., NOAA, Silver Spring, Md.

Liang, W.-D., T. Y. Tang, Y. J. Yang, M. T. Ko, and W.-S. Chuang (2003), Upper-ocean currents around Taiwan, *Deep Sea Res., Part II*, *50*, 1085–1105, doi:10.1016/S0967-0645(03)00011-0.

Liang, W.-D., Y. J. Yang, T. Y. Tang, and W.-S. Chuang (2008), Kuroshio in the Luzon Strait, *J. Geophys. Res.*, *113*, C08048, doi:10.1029/2007JC004609.

Liao, G., Y. Yuan, and X. Xu (2008), Three dimensional diagnostic study of the circulation in the South China Sea during winter 1998, *J. Oceanogr.*, *64*, 803–814, doi:10.1007/s10872-008-0067-4.

Mellor, G. L. (2004), Users guide for a three-dimensional, primitive equation, numerical ocean model, report, 56 pp., Princeton Univ. Program in Atmos. and Oceanic Sci., Princeton, N. J.

Metzger, E. J. (2003), Upper ocean sensitivity to wind forcing in the South China Sea, *J. Oceanogr.*, *59*, 783–798, doi:10.1023/B:JOCE.0000009570.41358.c5.

Metzger, E. J., and H. E. Hurlburt (1996), Coupled dynamics of the South China Sea, the Sulu Sea, and the Pacific Ocean, *J. Geophys. Res.*, *101*, 12,331–12,352, doi:10.1029/95JC03861.

Metzger, E. J., and H. E. Hurlburt (2001a), The importance of high horizontal resolution and accurate coastline geometry in modeling South China Sea inflow, *Geophys. Res. Lett.*, *28*, 1059–1062, doi:10.1029/2000GL012396.

Metzger, E. J., and H. E. Hurlburt (2001b), The nondeterministic nature of Kuroshio penetration and eddy shedding in the South China Sea, *J. Phys. Oceanogr.*, *31*, 1712–1732, doi:10.1175/1520-0485(2001)031<1712:TNNOKP>2.0.CO;2.

Oey, L.-Y., Y.-C. Hsin, and C.-R. Wu (2010), Why does the Kuroshio northeast of Taiwan shift shelfward in winter?, *Ocean Dyn.*, *60*, 413–426, doi:10.1007/s10236-009-0259-5.

Qiu, B. (1999), Seasonal eddy field modulation of the North Pacific Subtropical Countercurrent: TOPEX/POSEIDON observations and theory, *J. Phys. Oceanogr.*, *29*, 2471–2486, doi:10.1175/1520-0485(1999)029<2471:SEFMOT>2.0.CO;2.

Qiu, B., and R. Lukas (1996), Seasonal and interannual variability of the North Equatorial Current, the Mindanao Current, and the Kuroshio along the Pacific western boundary, *J. Geophys. Res.*, *101*, 12,315–12,330, doi:10.1029/95JC03204.

Qu, T. (2000), Upper-layer circulation in the South China Sea, *J. Phys. Oceanogr.*, *30*, 1450–1460, doi:10.1175/1520-0485(2000)030<1450:ULCITS>2.0.CO;2.

Qu, T., H. Mitsudera, and T. Yamagata (1999), A climatology of the circulation and water mass distribution near the Philippine coast, *J. Phys. Oceanogr.*, *29*, 1488–1505, doi:10.1175/1520-0485(1999)029<1488:ACOTCA>2.0.CO;2.

Qu, T., H. Mitsudera, and T. Yamagata (2000), Intrusion of the North Pacific waters into the South China Sea, *J. Geophys. Res.*, *105*, 6415–6424, doi:10.1029/1999JC900323.

Qu, T., Y. Y. Kim, M. Yaremchuk, T. Tozuka, A. Ishida, and T. Yamagata (2004), Can Luzon Strait transport play a role in conveying the impact of ENSO to the South China Sea?, *J. Clim.*, *17*, 3644–3657, doi:10.1175/1520-0442(2004)017<3644:CLSTPA>2.0.CO;2.

Qu, T., J. B. Girton, and J. A. Whitehead (2006a), Deepwater overflow across Luzon Strait, *J. Geophys. Res.*, *111*, C01002, doi:10.1029/2005JC003139.

Qu, T., Y. Du, and H. Sasaki (2006b), South China Sea throughflow: A heat and freshwater conveyor, *Geophys. Res. Lett.*, *33*, L23617, doi:10.1029/2006GL028350.

Rong, Z., Y. Liu, H. Zong, and Y. Cheng (2007), Interannual sea level variability in the South China Sea and its response to ENSO, *Global Planet. Change*, *55*, 257–272, doi:10.1016/j.gloplacha.2006.08.001.

Shaw, P.-T. (1989), The intrusion of water masses into the sea southwest of Taiwan, *J. Geophys. Res.*, *94*, 18,213–18,226, doi:10.1029/JC094iC12p18213.

Shaw, P.-T. (1991), The seasonal variation of the intrusion of the Philippine Sea water into the South China Sea, *J. Geophys. Res.*, *96*, 821–827, doi:10.1029/90JC02367.

Sheremet, V. A. (2001), Hysteresis of a western boundary current leaping across a gap, *J. Phys. Oceanogr.*, *31*, 1247–1259, doi:10.1175/1520-0485(2001)031<1247:HOAWBC>2.0.CO;2.

Sheu, W.-J., C.-R. Wu, and L.-Y. Oey (2010), Blocking and westward passage of eddies in the Luzon Strait, *Deep Sea Res., Part II*, *57*, 1783–1791, doi:10.1016/j.dsr.2010.04.004.

Song, Y. T. (2006), Estimation of interbasin transport using ocean bottom pressure: Theory and model for Asian marginal seas, *J. Geophys. Res.*, *111*, C11S19, doi:10.1029/2005JC003189.

Su, J., (2004), Overview of the South China Sea circulation and its influence on the coastal physical oceanography outside the Pearl River Estuary, *Cont. Shelf Res.*, *24*, 1745–1760, doi:10.1016/j.csr.2004.06.005.

Tian, J., Q. Yang, X. Liang, L. Xie, D. Hu, F. Wang, and T. Qu (2006), Observation of Luzon Strait transport, *Geophys. Res. Lett.*, *33*, L19607, doi:10.1029/2006GL026272.

Wajsowicz, R. C. (1999), Models of the Southeast Asian seas, *J. Phys. Oceanogr.*, *29*, 986–1018, doi:10.1175/1520-0485(1999)029<0986:MOTSAS>2.0.CO;2.

Wang, D., Q. Liu, R. X. Huang, Y. Du, and T. Qu (2006), Interannual variability of the South China Sea throughflow inferred from wind data and an ocean data assimilation product, *Geophys. Res. Lett.*, *33*, L14605, doi:10.1029/2006GL026316.

Wang, Q., H. Cui, S. Zhang, and D. Hu (2009), Water transports through the four main straits around the South China Sea, *Chin. J. Oceanol. Limnol.*, *27*, 229–236, doi:10.1007/s00343-009-9142-y.

Wijffels, S. E., G. Meyers, and J. S. Godfrey (2008), A 20-yr average of the Indonesian Throughflow: Regional currents and the interbasin exchange, *J. Phys. Oceanogr.*, *38*, 1965–1978, doi:10.1175/2008JPO3987.1.

Wu, C.-R., and T.-L. Chiang (2007), Mesoscale eddies in the northern South China Sea, *Deep Sea Res., Part II*, *54*, 1575–1588, doi:10.1016/j.dsr2.2007.05.008.

Wu, C.-R., and Y.-C. Hsin (2005), Volume transport through the Taiwan Strait: A numerical study, *Terr. Atmos. Oceanic Sci.*, *16*(2), 377–391.

Wu, C.-R., T. Y. Tang, and S. F. Lin (2005), Intra-seasonal variation in the velocity field of the northeastern South China Sea, *Cont. Shelf Res.*, *25*, 2075–2083, doi:10.1016/j.csr.2005.03.005.

Wu, C.-R., Y.-L. Chang, L.-Y. Oey, C.-W. J. Chang, and Y.-C. Hsin (2008), Air-sea interaction between tropical cyclone Nari and Kuroshio, *Geophys. Res. Lett.*, *35*, L12605, doi:10.1029/2008GL033942.

Wyrtki, K. (1961), *Physical Oceanography of the Southeast Asian Waters*, vol. 2, 195 pp., Scripps Inst. of Oceanogr., Univ. of Calif., La Jolla.

Xue, H., F. Chai, N. Pettigrew, D. Xu, M. Shi, and J. Xu (2004), Kuroshio intrusion of the circulation in the South China Sea, *J. Geophys. Res.*, *109*, C02017, doi:10.1029/2002JC001724.

Yang, Q., J. Tian, and W. Zhao (2010), Observation of Luzon Strait transport in summer 2007, *Deep Sea Res., Part I*, *57*, 670–676, doi:10.1016/j.dsr.2010.02.004.

Yaremchuk, M., and T. Qu (2004), Seasonal variability of the large-scale currents near the coast of the Philippines, *J. Phys. Oceanogr.*, *34*, 844–855, doi:10.1175/1520-0485(2004)034<0844:SVOTLC>2.0.CO;2.

Yaremchuk, M., J. McCreary Jr., Z. Yu, and R. Furue (2009), The South China Sea throughflow retrieved from climatological data, *J. Phys. Oceanogr.*, *39*, 753–767, doi:10.1175/2008JPO3955.1.

Yuan, Y., G. Liao, and C. Yang (2008a), The Kuroshio near the Luzon Strait and circulation in the northern South China Sea during August and September 1994, *J. Oceanogr.*, *64*, 777–788, doi:10.1007/s10872-008-0065-6.

Yuan, Y., G. Liao, W. Guan, H. Wang, R. Lou, and H. Chen (2008b), The circulation in the upper and middle layers of the Luzon Strait during spring 2002, *J. Geophys. Res.*, *113*, C06004, doi:10.1029/2007JC004546.

Yuan, Y., G. Liao, and C. Yang (2009), A diagnostic calculation of the circulation in the upper and middle layers of the Luzon Strait and the northern South China Sea during March 1992, *Dyn. Atmos. Oceans*, *47*, 86–113, doi:10.1016/j.dynatmoce.2008.10.005.

Zhao, W., Y.-J. Hou, P. Qi, K.-T. Le, and M.-K. Li (2009), The effects of monsoons and connectivity of South China Sea on the seasonal variations of water exchange in the Luzon Strait, *J. Hydrodyn.*, *21*, 264–270, doi:10.1016/S1001-6058(08)60144-4.

Zhou, H., F. Nan, M. Shi, L. Zhou, and P. Guo (2009), Characteristics of water exchange in the Luzon Strait during September 2006, *Chin. J. Oceanology Limnol.*, *27*(3), 650–657, doi:10.1007/s00343-009-9175-2.

Zhuang, W., S.-P. Xie, D. Wang, B. Taguchi, H. Aiki, and H. Sasaki (2010), Intraseasonal variability in sea surface height over the South China Sea, *J. Geophys. Res.*, *115*, C04010, doi:10.1029/2009JC005647.

S.-Y. Chao, Horn Point Laboratory, University of Maryland Center for Environmental Science, PO Box 775, Cambridge, MD 21613, USA.

Y.-C. Hsin, Department of Oceanography, University of Hawaii at Mānoa, 1000 Pope Rd., Honolulu, HI 96822, USA. (yichia@hawaii.edu)

C.-R. Wu, Department of Earth Sciences, National Taiwan Normal University, 88, Section 4 Ting-Chou Rd., Taipei 11677, Taiwan. (cwu@ntnu.edu.tw)